CHAPTER 4

CURE CHARACTERISTICS AND MECHANICAL BEHAVIOUR OF UNFILLED AND FILLED NBR/EVA BLENDS

The results of this chapter have been submitted for publication in *J. Appl. Polym. Sci.*

Commercial products have been based on miscible[1-3] as well as immiscible blends.[4,5] For blends of immiscible polymers, the mechanical response reflects molecular relaxation processes characteristic of each constituent and is also profoundly influenced by blend composition, morphology and peculiar relaxation processes characteristic of the blend. The morphological arrangement may consist of one phase dispersed in a matrix of the other polymer.

Homogeneity of mixing and cure compatibility are the most pertinent polymeric properties related to polymer blends. Homogeneity at a microscopic level is necessary for optimum performance but some degree of micro-heterogeneity is usually desirable to preserve the individual properties of the respective polymer components. Even if true miscibility may not be required, adhesion between polymer phases is necessary for good properties. Shershnev[6] summarised the importance of and requirements for covulcanisation of the components of elastomer blends. Covulcanisation is defined in terms of a single network structure with crosslinked macromolecules of both polymers. Vulcanisates with components having similar curative reactivity generally give better properties than those whose components have large differences in this regard. To select a blend ratio and a crosslinking system suitable for a particular application, a clear understanding of the change in properties with blend ratio and crosslinking systems is essential.

Usually reinforcement in rubber compounds is achieved by the use of black as well as non-black fillers. Fillers are used to modify the processing characteristics, mechanical properties and also to reduce the cost. Further, fillers reduce the shrinkage and increase the modulus and hardness of rubber compounds. The reinforcement of the filler in blends depends on the affinity of the filler towards the blend components and also on the distribution and dispersion of filler in each phase of the blend. The filler interphase distribution in elastomer blends has been reported by several researchers.[7-10] In the selection of a polymer system for practical applications one has to consider how the material can resist failure or crack growth under the use conditions. In order to have an insight into the resistance of the material to failure or crack growth, it is essential to carry out the mechanical property measurements. The mode of failure of a material can be investigated using a scanning electron microscope and the failure pattern can be related to the strength of the material.

In this chapter, the effects of crosslinking systems, blend ratio and various fillers on the mechanical properties and failure mechanism of NBR/EVA blends are dealt with. Dicumyl peroxide has been used for crosslinking both NBR and EVA. But sulphur can crosslink only NBR phase and not EVA due to its saturated backbone structure. Hence a mixed system, containing both peroxide and sulphur, was also selected for the effective curing of both the phases in the blend. In fact mixed and peroxide systems give rise to full interpenetrating networks, while sulphur cure system leads to a semi-interpenetrating network.

4.1 Results and discussion

4.1.1 Morphology

The polymer blend properties are strongly influenced by the morphology of the system. Several researchers[11-14] have related the variation in properties with the blend morphology. The morphology of the crosslinked systems of the different blend compositions is speculated based on the morphology of uncrosslinked systems and is shown in Figure 4.1. In fact the analysis of morphology by SEM was impossible since both phases are crosslinked.

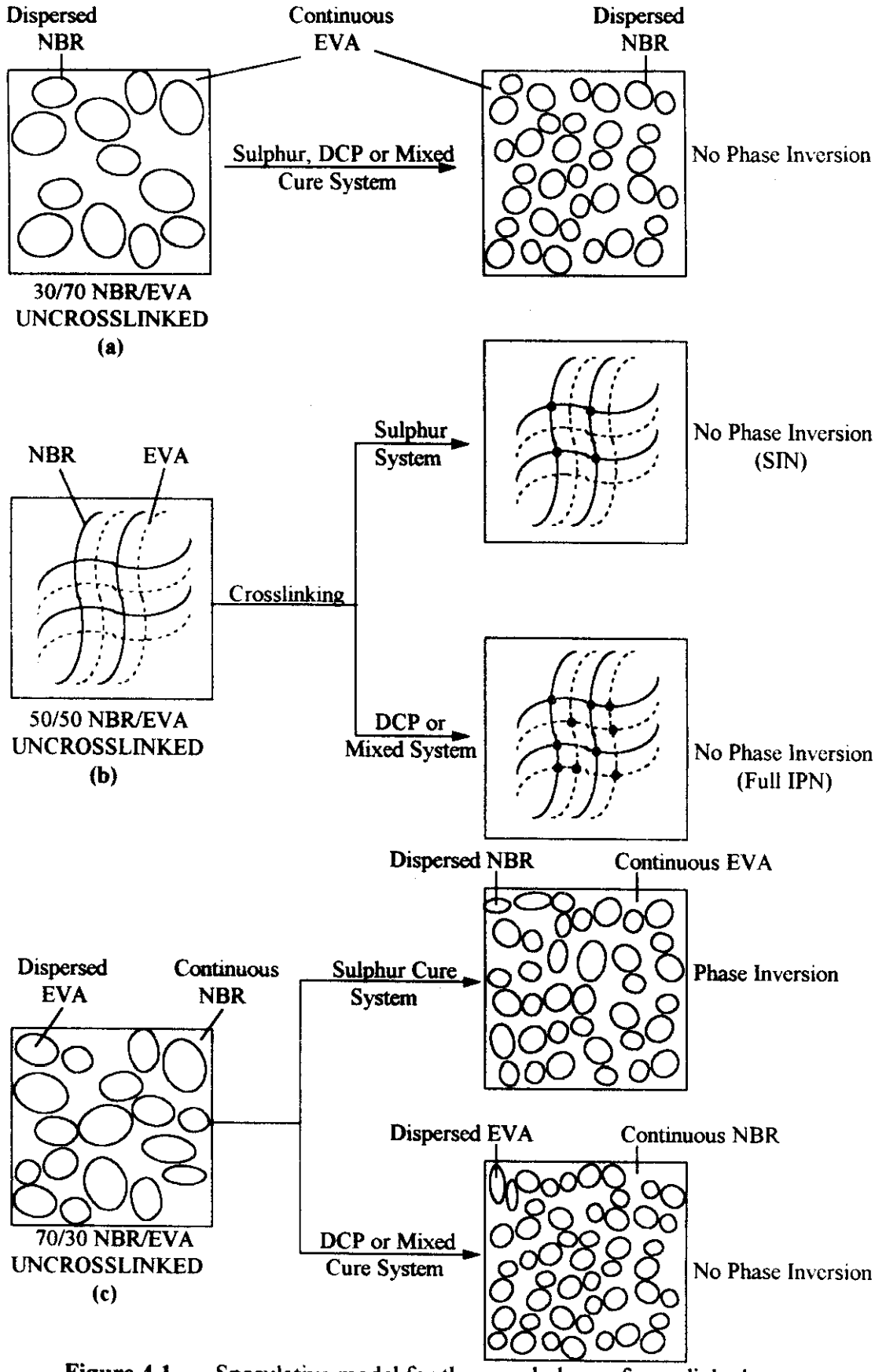

Figure 4.1. Speculative model for the morphology of crosslinked systems

When N_{30} (Figure 4.1a) is crosslinked, a particle size reduction is expected for the dispersed NBR phase. In N_{50} (Figure 4.1b) when sulphur is the curing agent, only NBR is crosslinked and results in the formation of a semi-interpenetrating network. For the peroxide and mixed cure systems, both the phases are crosslinked and results in the formation of a full-interpenetrating network. In N_{70} (Figure 4.1c), a phase inversion is expected for the sulphur cured system and the crosslinked NBR particles are dispersed in the continuous EVA matrix. For the other two crosslinking systems, there is no phase inversion.

4.1.2 Cure characteristics

The cure characteristics of the crosslinked and filled NBR/EVA blends are given in Table 4.1. The mixed cure system exhibits highest cure time and the peroxide cure system, where the cure reaction occurs by free radical mechanism, exhibits the lowest cure time. In all the cure systems, the cure time decreases with the increase in NBR content. The scorch safety is highest for the sulphur cure system and lowest for the peroxide cure system. Maximum torque, which is a measure of crosslink density, is also given in the table. The maximum torque is higher for EVA (N_0) and EVA rich blends than that of the other blend compositions.

The filled systems exhibit slightly higher cure time than that of the unfilled one ($N_{50}P$). This is probably due to the adsorption of the curatives on the surface of the fillers. From Table 4.1 it is observed that the scorch time of the blend is not affected on the addition of fillers. However, fillers are found to increase the maximum torque which is dependent on the level of loading. This is attributed to the increased modulus of the filled vulcanisates. The rheographs of a few mixes are given in Figure 4.2 and it can be seen that the compounds do not show any tendency for reversion.

Table 4.1. Cure characteristics of NBR/EVA systems at 160°C

Sample code	Cure time (min)	Scorch time (min)	Max. torque (dNm)	CRI*
N_0P	24.0	2.0	80.2	4.5
$N_{30}P$	20.0	3.0	70.1	5.8
$N_{50}P$	18.4	2.5	49.9	6.3
$N_{70}P$	17.2	2.2	35.1	6.7
$N_{100}P$	16.5	2.1	39.2	6.9
$N_{30}S$	32.0	20.0	61.9	8.3
$N_{50}S$	19.0	13.0	51.9	1637
$N_{70}S$	19.4	11.0	38.1	11.9
$N_{100}S$	14.4	7.2	19.2	13.9
N_0M	40.0	18.0	66.4	4.5
$N_{30}M$	34.0	9.4	71.4	4.1
$N_{50}M$	27.0	5.8	52.9	4.7
$N_{70}M$	17.8	5.0	43.5	7.8
$N_{100}M$	18.8	3.6	22.1	6.6
10S	18.6	2.1	82.5	6.1
10C	18.7	1.9	83.1	5.9
10BS	19.1	2.4	83.5	5.9
20BS	19.0	2.2	89.8	5.9
30BS	19.2	2.2	93.2	5.8
10BH	19.4	2.3	84.7	5.8
20BH	19.2	2.1	90.5	5.8
30BH	19.3	2.0	94.9	5.8

*CRI - cure rate index

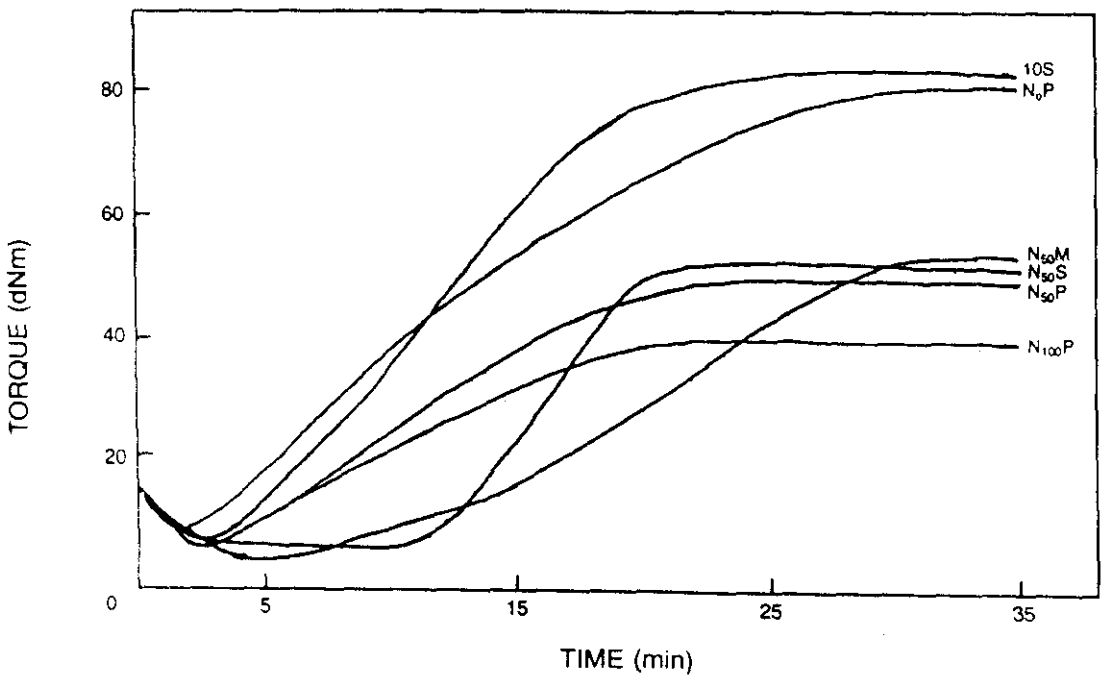

Figure 4.2. Rheographs of NBR/EVA blends

Cure rate index (CRI) is calculated using the equation:

$$CRI = 100/t_{90}-t_2 \qquad (4.1)$$

where t_{90} is the optimum cure time and t_2 is the scorch time. The CRI values are given in Table 4.1. In all the crosslinking systems, the cure rate index increases with the increase in NBR content. Thus NBR is the cure activating component in this system. A high CRI value indicates a higher vulcanisation rate. All the filled systems exhibit nearly same CRI values.

4.1.3 Mechanical properties

The stress-strain curves of the peroxide crosslinked systems for the different blend compositions are shown in Figure 4.3.

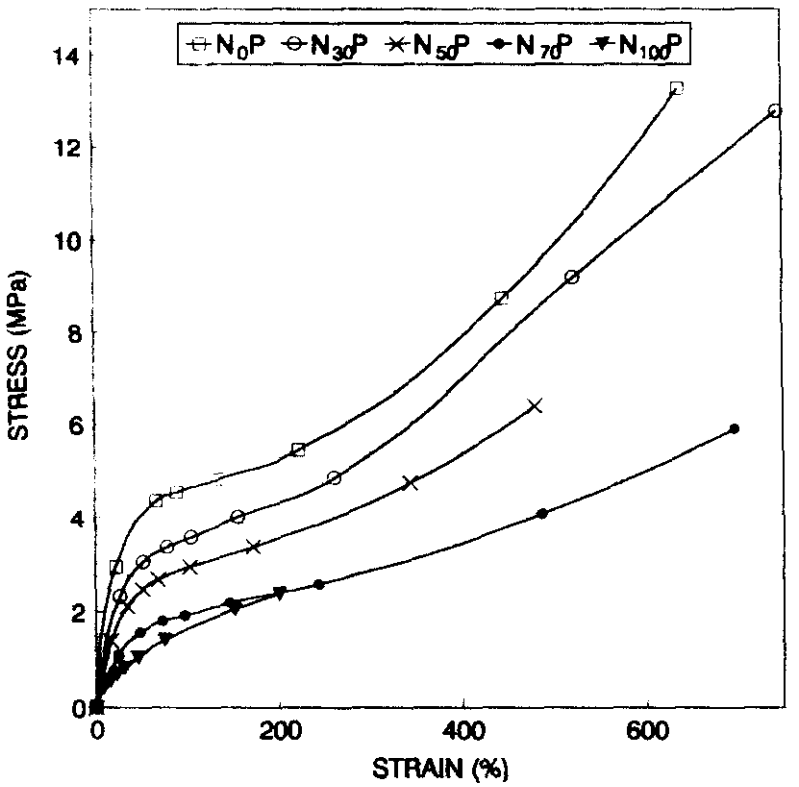

Figure 4.3. Stress-strain curves of peroxide cured NBR/EVA blends

An increase in the initial modulus is observed with increase in EVA content of the blend. Thus NBR ($N_{100}P$) shows the lowest modulus and fails at fairly low stress. As the EVA content in the blend increases, there is an increase in the stress with increasing strain. This is due to the orientation of the crystalline regions of EVA in the direction of force. The effect of different crosslinking systems, viz., sulphur (S), dicumyl peroxide (P) and the mixed (M) systems on the stress-strain behaviour of NBR/EVA blends are given in Figures 4.4–4.6. All the systems show very similar stress-strain behaviour and the initial modulus values lie close to each other. However, the peroxide cured system takes the lowest position. The difference is too marginal in the case of N_{30} and N_{50} but it is predominant in the case of N_{70}.

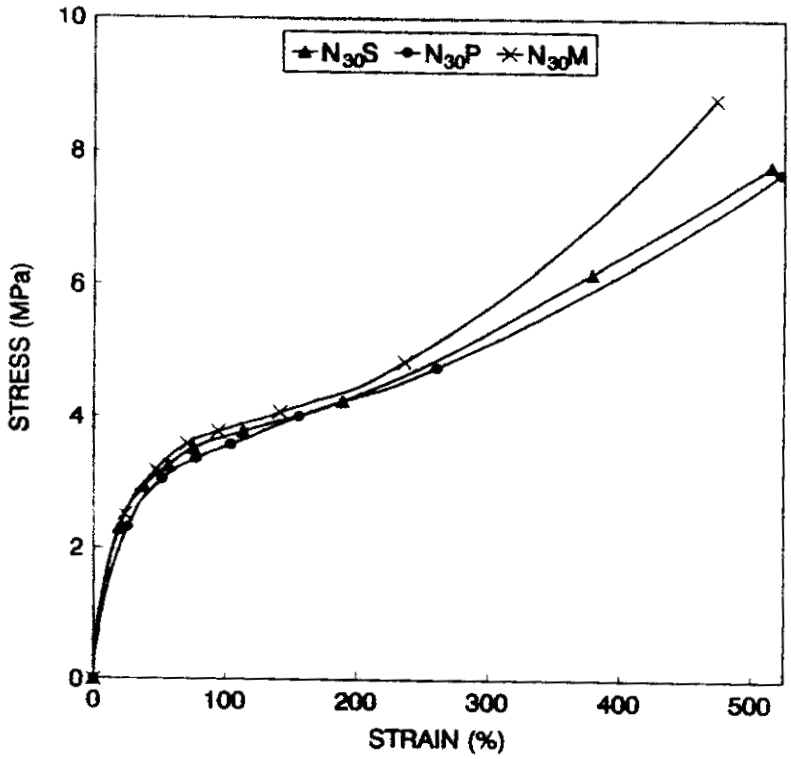

Figure 4.4. Effect of different crosslinking systems on the stress-strain behaviour of 30/70: NBR/EVA blend

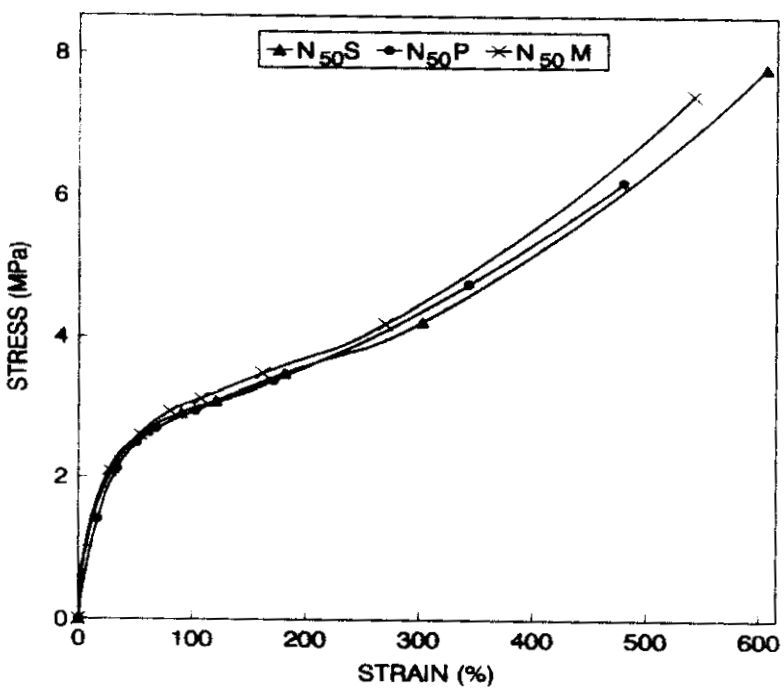

Figure 4.5. Effect of different crosslinking systems on the stress-strain behaviour of 50/50: NBR/EVA blend

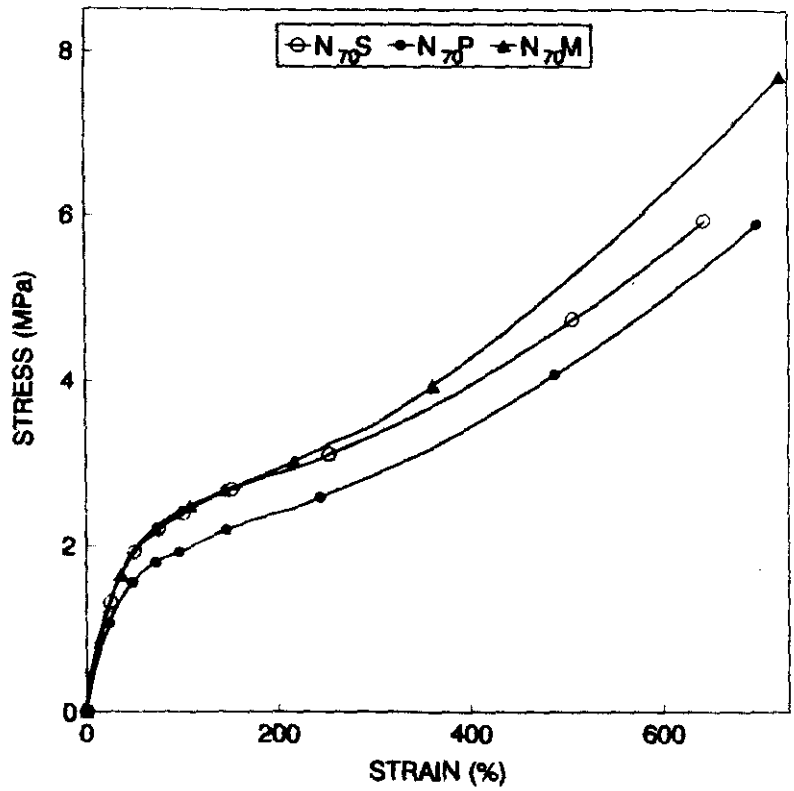

Figure 4.6. Effect of different crosslinking systems on the stress-strain behaviour of 70/30: NBR/EVA blend

It is possible to relate the properties with respect to the structure of the network formed. A schematic representation of the nature of crosslinks in the different cured system is given in Figure 4.7. The bond lengths for C-C, C-S and S-S linkages are 1.54, 1.81 and 1.88 Å, respectively, i.e., the C-C linkages are short and rigid. Under an applied load the rigid C-C linkages break easily compared to the flexible C-S and S-S linkages. The highly flexible and labile linkages are capable of withstanding a higher stress. The polysulphidic estimation was carried out in the case of $N_{50}S$ and $N_{50}M$, and it was found that the polysulphidic crosslinks are 55 and 45% respectively.

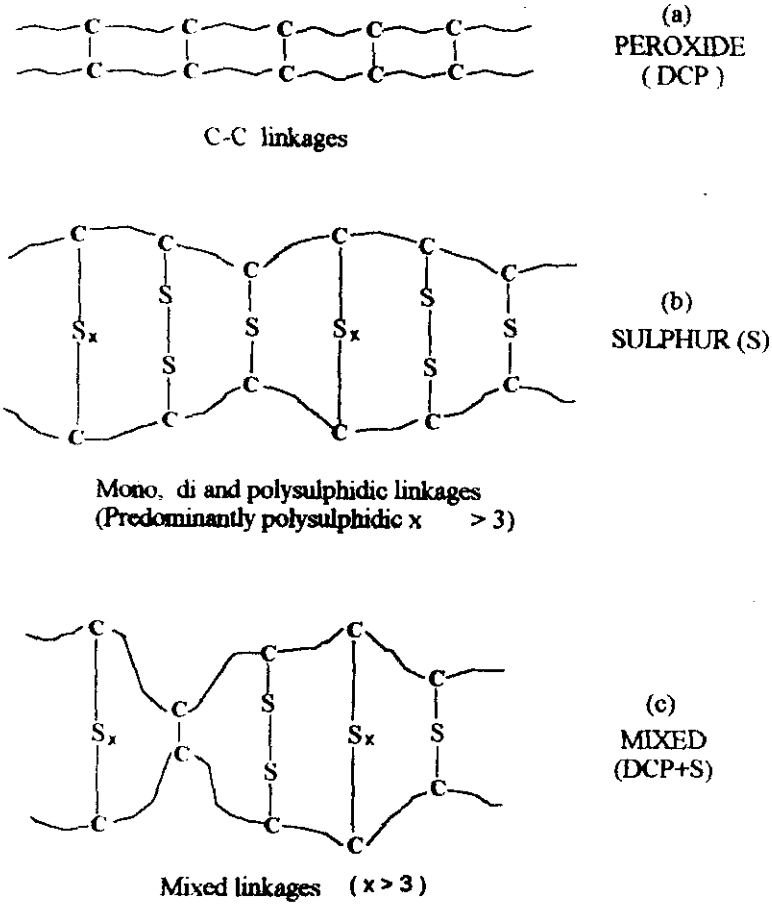

Figure 4.7. A schematic representation showing the nature of crosslinks in various crosslinking systems

Figure 4.8 shows the variation in tensile strength with the weight percentage of EVA in the blend. In the case of peroxide and mixed systems, the tensile strength increases with the increase in EVA content. But in the case of sulphur cured system there is a drop in tensile strength beyond 50% of EVA content. This is due to the phase inversion in morphology of the system. As shown in Section 3.1.1 beyond 50% EVA content, EVA is the continuous phase which cannot be crosslinked by sulphur. Thus in EVA rich blends, the continuous phase remains uncrosslinked when sulphur is the curing agent. Hence the drop in tensile strength beyond 50% of EVA content.

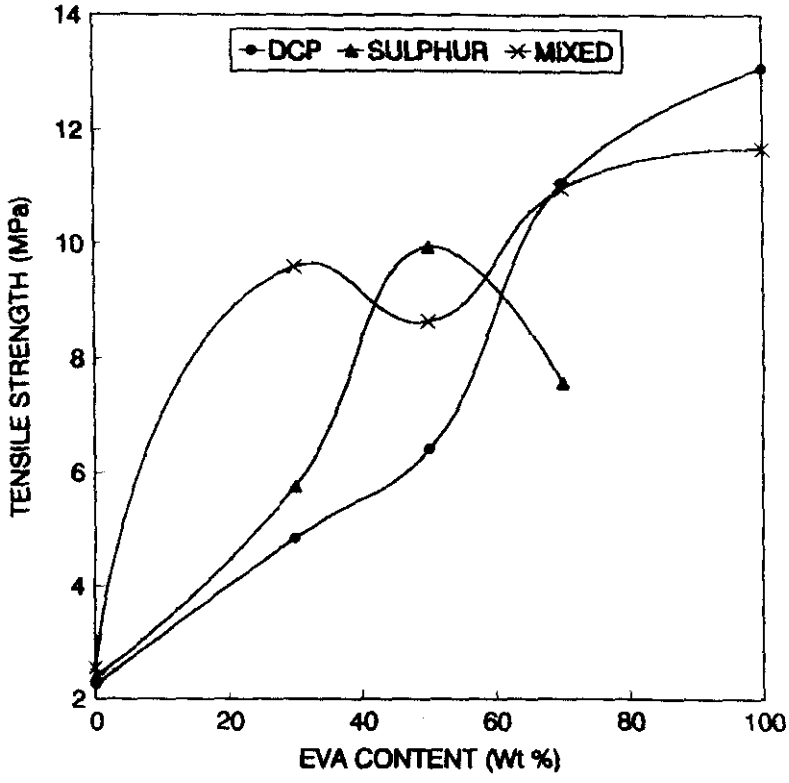

Figure 4.8. Variation in tensile strength with the weight percentage of EVA

The crosslink density of the samples was calculated from the tensile measurements using the equation (2.4). The values of Young's modulus, crosslink density and tensile set are given in Table 4.2. It is seen that the peroxide cured systems show comparatively lower Young's moduli compared to those of the other curing systems. It is also seen that the Young's modulus increases with the increasing EVA content in the blend. The peroxide cured systems of the pure components i.e., N_0P and $N_{100}P$ show higher crosslink density. But in the case of blends the mixed cure system shows slightly higher crosslink density. The samples with a high crosslink density exhibit lower tensile set. The set value decreases with increasing NBR content. A low set value is technologically advantageous.

Table 4.2. Mechanical properties of crosslinked and filled NBR/EVA blends

Sample code	Young's modulus (MPa)	Tensile set (%) (after failure)	Crosslink density ($\times 10^4$) gmol/cc
N_0P	14.8	3.50	3.69
N_0M	24.1	4.40	2.88
$N_{30}S$	12.7	1.40	2.62
$N_{30}P$	9.9	2.05	3.02
$N_{30}M$	13.9	1.45	3.11
$N_{50}S$	7.3	0.95	2.27
$N_{50}P$	6.6	0.75	2.18
$N_{50}M$	8.2	0.85	2.31
$N_{70}S$	4.8	0.70	1.67
$N_{70}P$	3.1	1.05	1.44
$N_{70}M$	4.6	0.55	1.89
$N_{100}S$	1.4	0.10	0.77
$N_{100}P$	1.9	0.05	1.68
$N_{100}M$	1.5	0.05	0.94
10S	9.4	0.55	5.54
10C	8.1	0.40	5.23
10BS	7.9	0.35	5.59
20BS	8.9	0.30	6.73
30BS	9.5	0.20	7.86
10BH	8.3	0.45	6.44
20BH	8.5	0.25	7.52
30BH	9.7	0.20	8.57

The dependence of elongation at break on the weight percentage of EVA for different cure systems is shown in Figure 4.9. The elongation at break monotonically increases with the increase in EVA content for DCP and mixed cure systems. In the case of sulphur cured system, N_{50} exhibits a maximum. The variations in hardness and tear strength with the weight percentage of EVA are presented in Figures 4.10 and 4.11 respectively. In both cases the property increases with the increase in EVA content in the blend. The mechanical

properties of NBR/EVA blends depend on the strength of EVA, which in turn depends on the crystallinity of EVA.

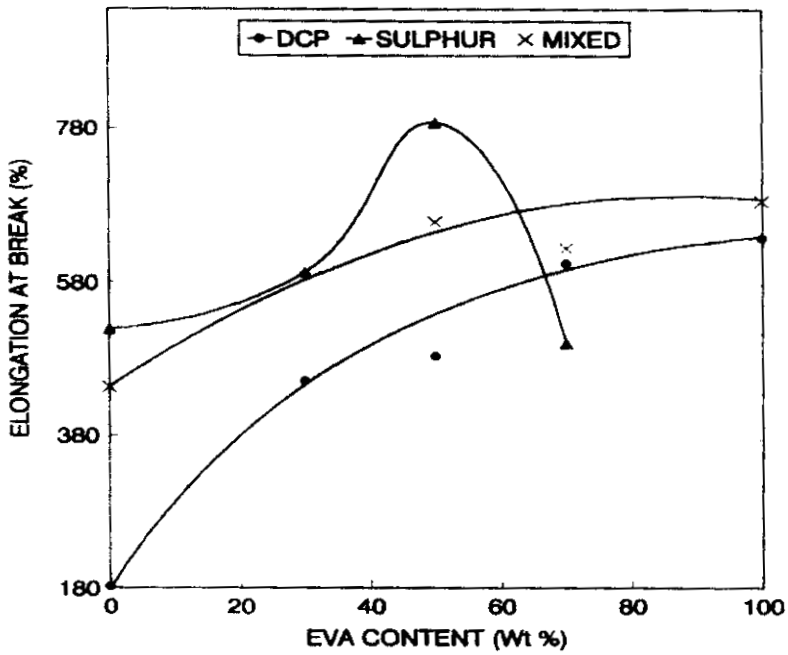

Figure 4.9. Variation in elongation at break with the weight percentage of EVA

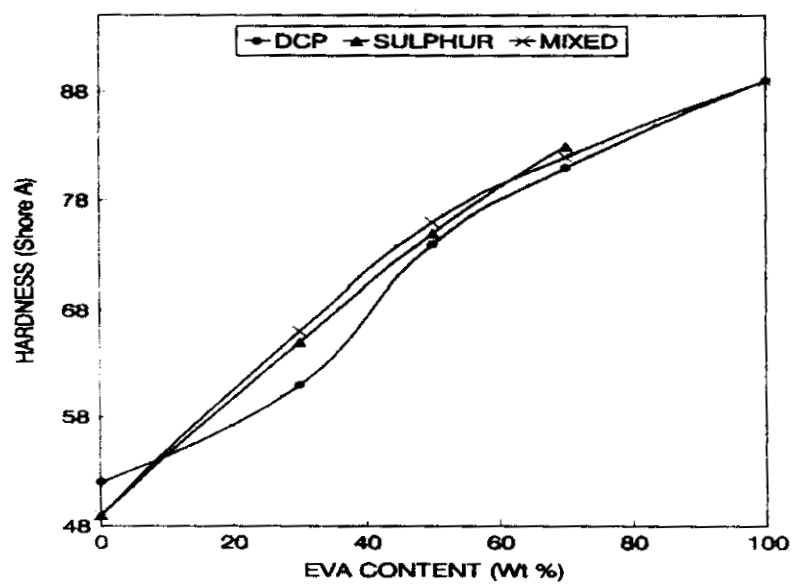

Figure 4.10. Variation in hardness with the blend ratio and crosslinking systems of NBR/EVA blends

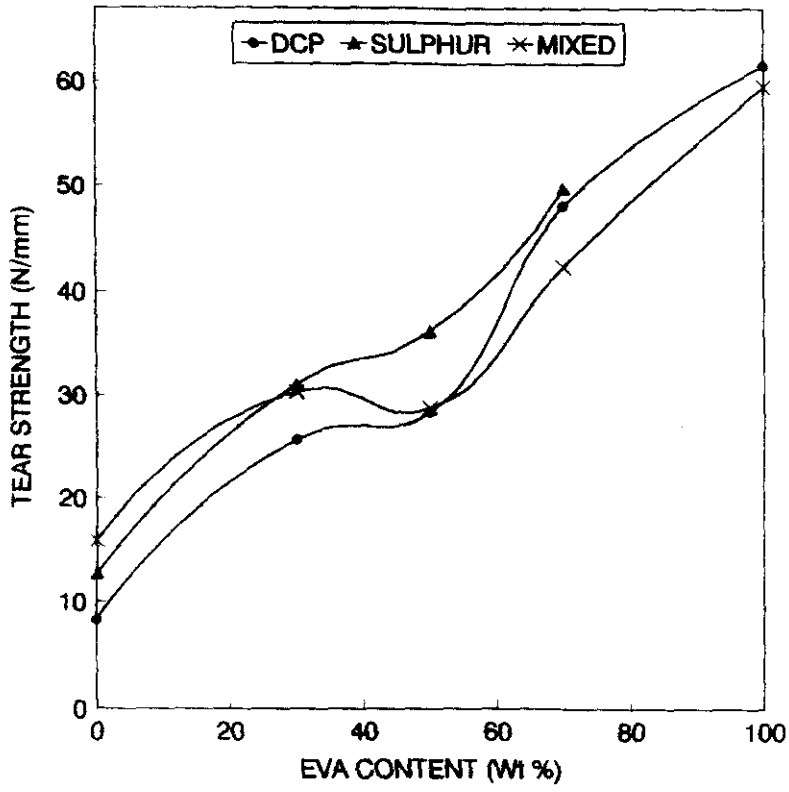

Figure 4.11. Variation in tear strength with the weight percentage of EVA

The tear curves (load vs. displacement) of the crosslinked NBR/EVA blends are given in Figures 4.12 and 4.13. The effect of blend ratio on the tear curves is shown in Figure 4.12. It is seen that EVA requires the highest load for tearing. The tearing force of EVA i.e., N_0P is followed by $N_{30}P$, $N_{50}P$, $N_{70}P$ and finally $N_{100}P$. i.e., NBR tears with the lowest load. This can be attributed to the drop in crystallinity with the increase in NBR content. In Figure 4.13, the tear curves of various cure systems are given. Here the peroxide cured system require the lowest load to tear. This is due to the nature of crosslinks (Figure 4.7) as explained earlier.

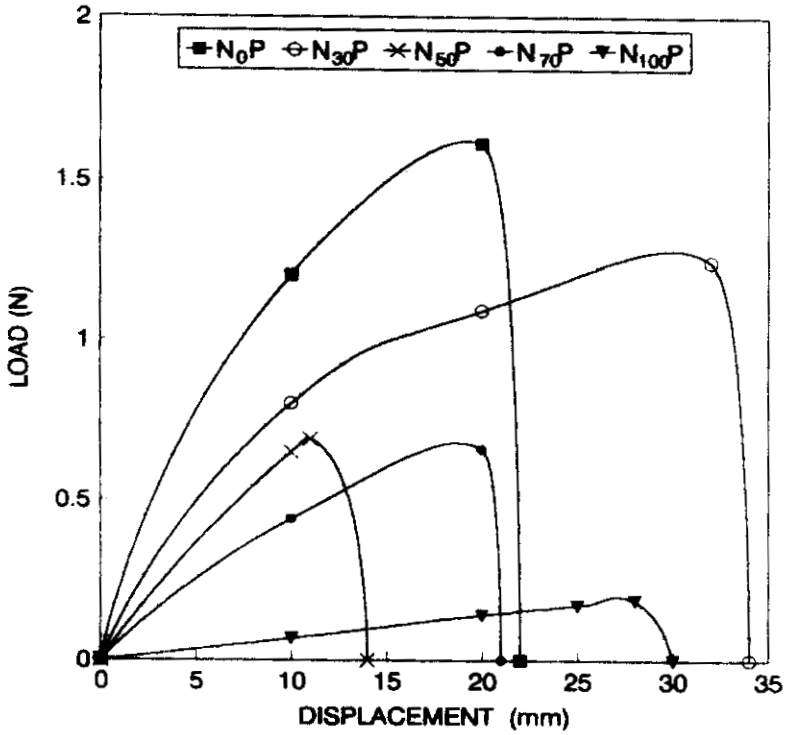

Figure 4.12. Effect of blend ratio on the tear curves of peroxide cured NBR/EVA blends

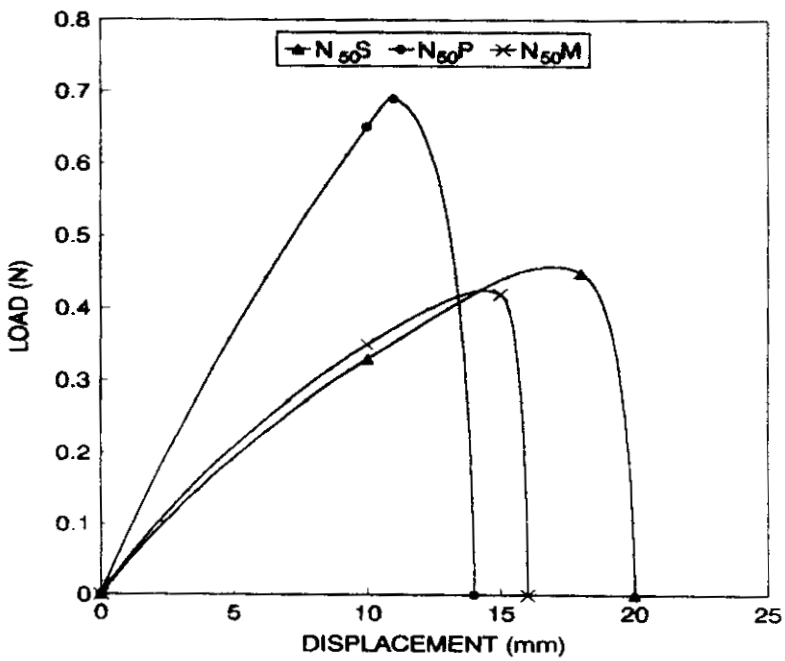

Figure 4.13. Effect of various crosslinking systems on the tear curves of NBR/EVA blends

4.1.4 *Scanning electron microscopic studies*

Scanning electron microscopy has been successfully used by several researchers to understand the failure mechanism in polymer blends.[15-20] The scanning electron micrographs of the tensile fracture surfaces of peroxide cured NBR/EVA blends are shown in Figure 4.14. Figures 4.14a–4.14c show the tensile fracture surfaces of N_0P, $N_{50}P$ and $N_{100}P$ respectively. N_0P exhibits a number of cracks on the fracture surface probably due to the disruption of crystallinity of EVA. $N_{50}P$ shows characteristic of ductile failure with a rough surface and that of $N_{100}P$ exhibits a smooth failure surface which is characteristic of rubbers.

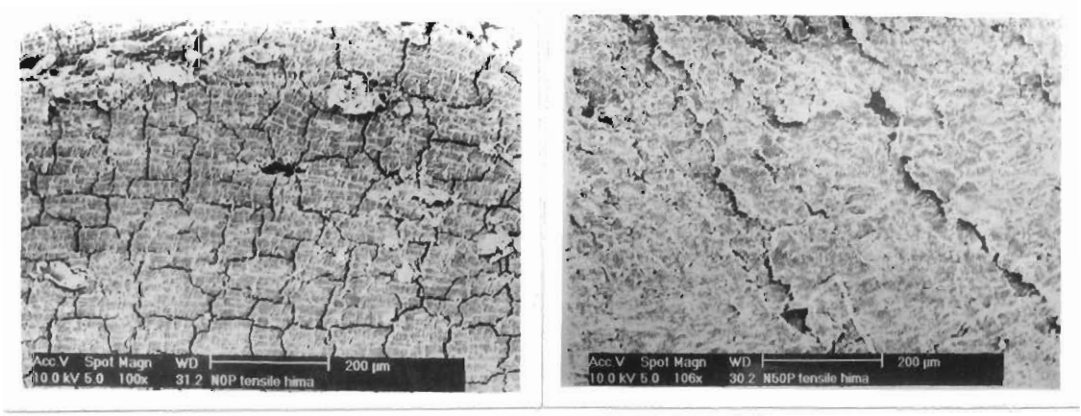

(a) (b)

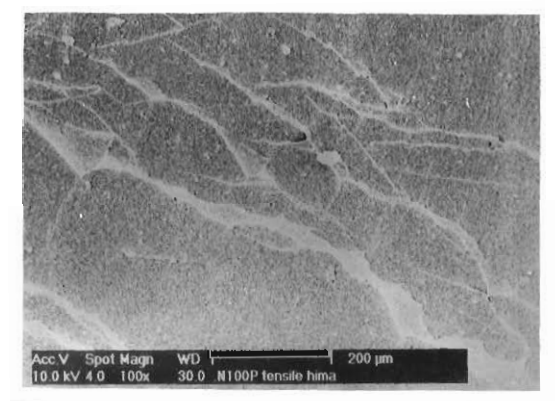

(c)

Figure 4.14. Scanning electron micrographs showing the tensile fracture surfaces of (a) N_0P, (b) $N_{50}P$ and (c) $N_{100}P$

The tear fractographs of peroxide crosslinked NBR/EVA blends are shown in Figure 4.15.

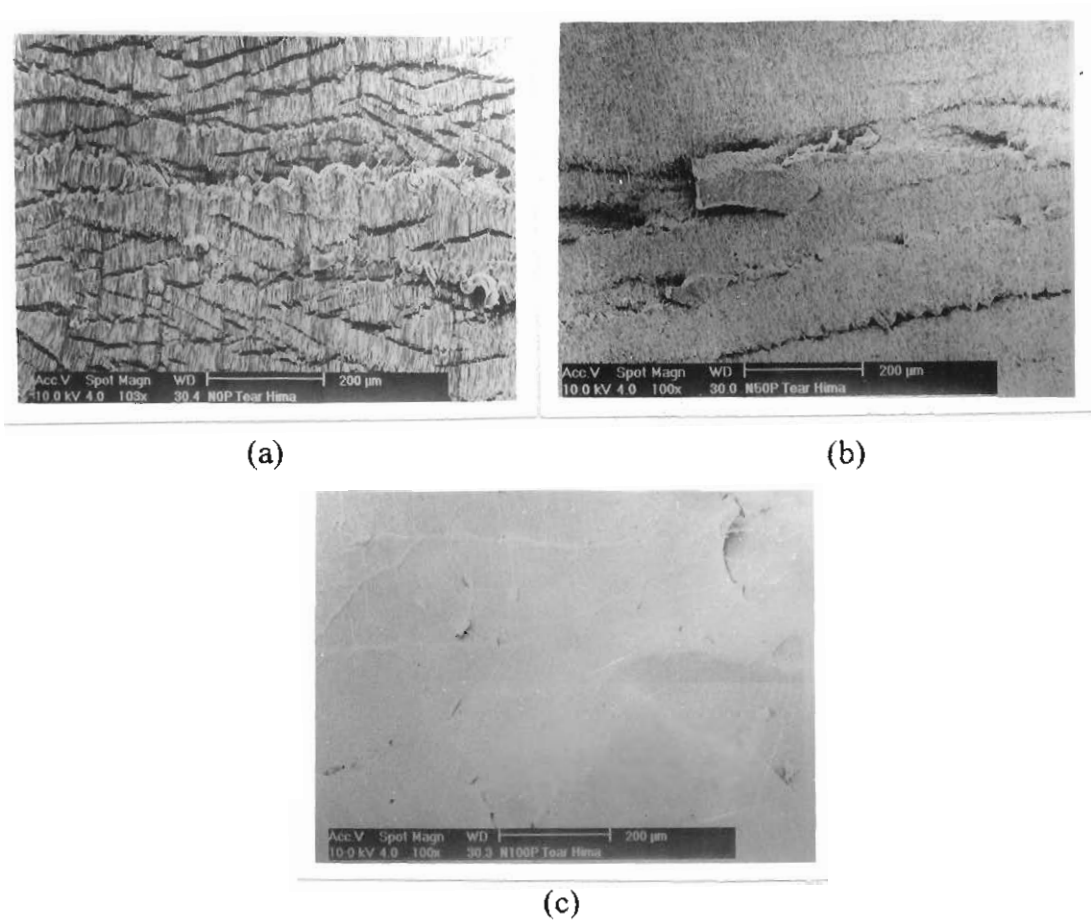

Figure 4.15. Scanning electron micrographs showing the tear fracture surfaces of (a) N_0P, (b) $N_{50}P$ and (c) $N_{100}P$

The fracture surface of N_0P (Figure 4.15a) shows tear fronts progressing sinusoidally with folds and striations which are characteristic of tear resistant materials. The spacing between the folds is estimated to be approximately 25 µm. Also, it is seen that there are several such sinusoidal tear fronts which lie close to each other. Sinusoidal tear fronts are also observed in $N_{50}P$ (Figure 4.15b). Here the spacing between the folds is approximately 35 µm. The increase in the step spacing between the folds indicate the drop in tear strength of the material. Gent and Pulford[15] related the step spacing to the tear strength of polymers. They measured the step spacing on the fracture surface and found that strong materials

show more closely spaced steps. As shown in Figure 4.15c, $N_{100}P$ exhibits smooth fracture surface characteristic of weak materials.

4.1.5 Model fitting

Applicability of various composite models such as parallel, series, Halpin-Tsai, Coran's, Takayanagi, Kerner and Kunori is examined to predict the mechanical behaviour of the blends. Details of all the equations are given in Section 3.1.3.

Comparison of experimental data and prediction using various models for tensile strength and modulus data is presented in Figures 4.16 and 4.17. In the case of tensile strength (Figure 4.16), the experimental value of N_{30} lies close to the parallel model. As the weight per cent of NBR increases, the experimental values deviate from the parallel model and are close to the Coran's model. In the case of Young's modulus (Figure 4.17), the experimental values are in good agreement with the Kerner model.

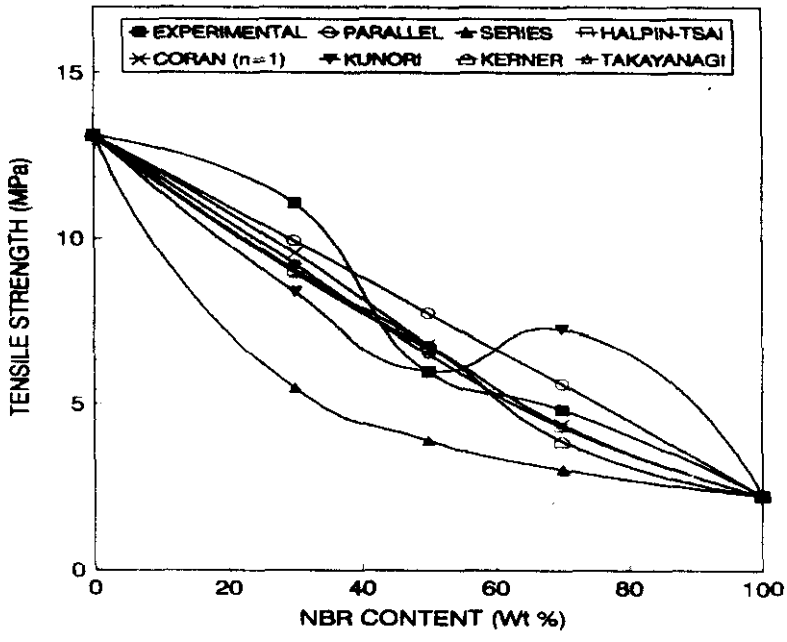

Figure 4.16. Applicability of various models on the tensile strength of peroxide cured NBR/EVA blends

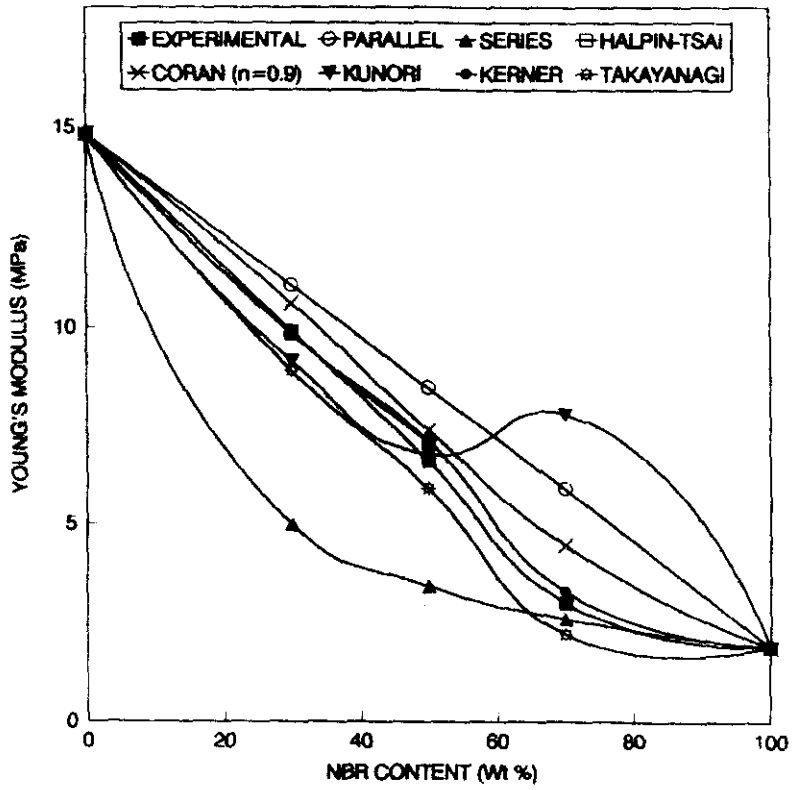

Figure 4.17. Applicability of various models on the Young's modulus of peroxide cured NBR/EVA blends

4.1.6 Effect of fillers

In order to study the effect of fillers, the peroxide cured 50/50:NBR/EVA blend ($N_{50}P$) is selected. The fillers used are silica, clay, semi-reinforcing furnace black (SRF) and high abrasion furnace black (HAF). The loading is kept constant, i.e., 10 phr, to compare the effect of different fillers. The effect of loading is studied using SRF and HAF. The reinforcement in blends depends on the filler interphase distribution i.e., the affinity of the filler towards the blend components. Generally in thermoplastic elastomers, the fillers are preferably located in the rubber phase [21]

(a) Extent of reinforcement

The extent of reinforcement is assessed by using Kraus equation.[22] According to this equation:

$$V_{r0}/V_{rf} = 1 - m\,(f/1-f) \tag{4.2}$$

where V_{rf} is the volume fraction of rubber in the solvent swollen filled sample and is given by the equation:

$$V_{rf} = \frac{(d - fw)\rho_p^{-1}}{(d - fw)\rho_p^{-1} + A_s\rho_s^{-1}} \tag{4.3}$$

where d is the deswollen weight; f, the volume fraction of the filler; w, the initial weight of the sample; ρ_p, the density of the polymer; ρ_s, the density of the solvent and A_s, the amount of solvent absorbed. For an unfilled system, f = 0. Substituting this in equation (4.3), the expression for the volume fraction of rubber in the solvent swollen unfilled sample (V_{r0}) is obtained.

$$V_{rf} = \frac{d\rho_p^{-1}}{d\rho_p^{-1} + A_s\rho_s^{-1}} \tag{4.4}$$

Since equation (4.2) has the general form of an equation for a straight line, a plot of V_{r0}/V_{rf} as a function of f/(1–f) should give a straight line, whose slope will be a direct measure of the reinforcing ability of the filler used. According to the theory developed by Kraus[22] for highly reinforcing carbon blacks, negative higher slope values indicate a better reinforcement. A constant C, characteristic of the filler is also calculated using the equation:

$$C = \frac{m - V_{r0} + 1}{3\left(1 - V_{r0}^{1/3}\right)} \tag{4.5}$$

The Kraus plots for various fillers are shown in Figure 4.18 and the values of slope and C are given in Table 4.3. It is observed that the amount of solvent absorbed (A_s) decreases as the filler loading increases. This results in an increase of the

V_{rf} values (with filler loading) calculated using equation (4.4). Since V_{r0} remains constant, the ratio V_{r0}/V_{rf} decreases with the filler loading, resulting in a negative slope (Figure 4.18). It is observed that the negative slope values which are a direct measure of the reinforcing ability of the fillers decreases in the order of HAF > SRF > silica > clay. This shows that as far as the extent of reinforcement is concerned, HAF is superior to other fillers.

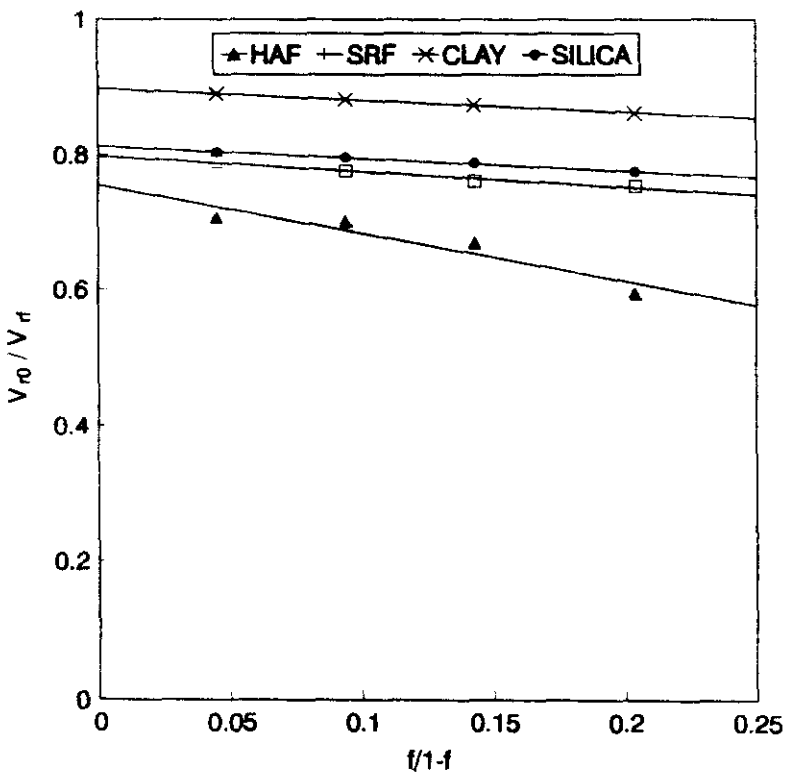

Figure 4.18. Plots of V_{r0}/V_{rf} vs. f/1-f for $N_{50}P$

Table 4.3. Values of negative slope and C for filled $N_{50}P$

Fillers	Negative slope	C
HAF	0.72	1.44
SRF	0.23	0.94
Silica	0.19	0.90
Clay	0.17	0.88

(b) Mechanical properties

The stress-strain curves of $N_{50}P$ with different fillers at 10 phr loading are compared in Figure 4.19. For a given strain, filled systems exhibit higher stress than the unfilled polymer blend. A considerable increase in stress with strain is observed beyond the yield stress for the filled systems. Among the different filled systems, the clay filled system exhibits a low failure stress. This is due to the low reinforcing ability of clay. The stress-strain curves of the HAF loaded $N_{50}P$ for various loadings are compared in Figure 4.20. For a given strain, the stress increases with increase in loading. This is due to the better reinforcement at higher loadings.

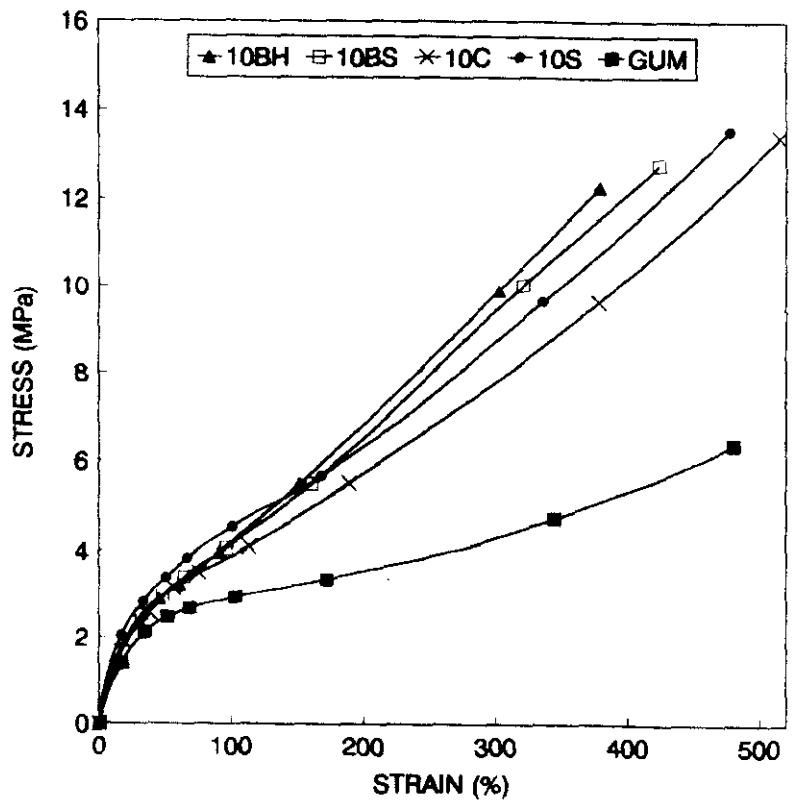

Figure 4.19. Effect of various fillers on the stress-strain behaviour of $N_{50}P$

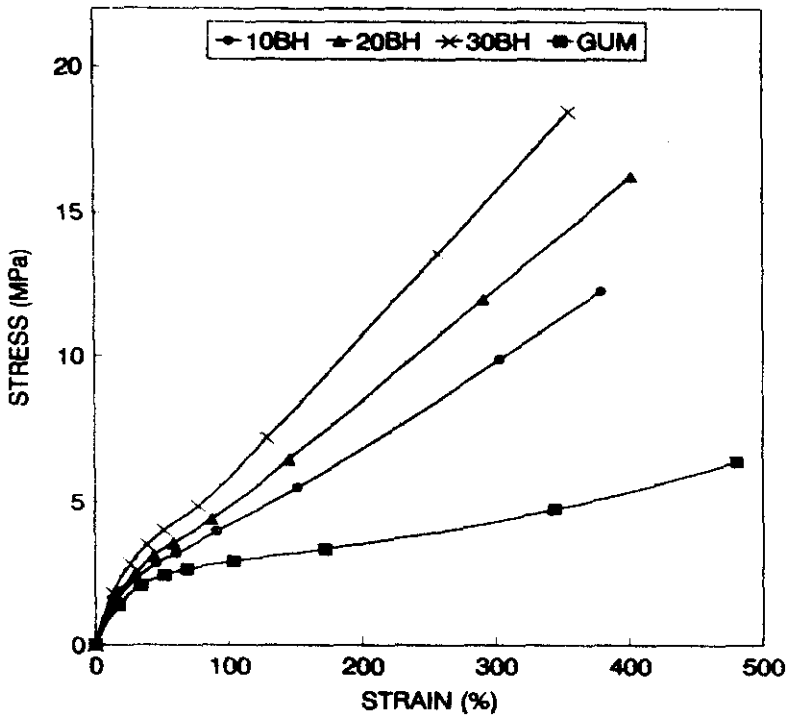

Figure 4.20. Effect of filler loading on the stress-strain behaviour of $N_{50}P$

The effect of fillers at 10 phr loading on the mechanical properties of $N_{50}P$ is given in Table 4.4. It is observed that the tensile strength, hardness and tear strength are increased with the addition of fillers. The propagation of the tear path is obstructed by the filler particles and hence the tear strength is increased with the addition of fillers. The tensile strength and tear strength are the highest for HAF filled system and lowest for the clay filled system. SRF and silica filled systems show intermediate values. The variation in properties of the different filled systems are in accordance with reinforcing ability of the filler as established by Kraus analysis. The elongation at break is decreased with the addition of black fillers and is almost unaffected by the addition of white fillers. Here the reduction in the elongation at break is more predominant for the highly reinforcing HAF black. An improvement in tensile set is observed with the addition of fillers (Table 4.2).

Table 4.4. Effect of fillers on the mechanical properties of $N_{50}P$

Property	Fillers (10 phr loading)				
	Gum	Silica	Clay	SRF	HAF
Tensile strength (MPa)	5.9	12.2	11.5	11.9	12.9
Elongation at break (%)	460	480	480	420	380
Hardness (Shore A)	74	80	76	76	77
Tear strength (N/mm)	24.4	34.1	25.4	32.5	34.9

The variation in properties of $N_{50}P$ with filler loading is depicted in Figures 4.21–4.24. It can be seen that the tensile strength (Figure 4.21), hardness (Figure 4.23), and tear strength (Figure 4.24) increase with loading for both the HAF and SRF filled systems. A reduction is observed in the case of elongation at break with loading (Figure 4.22).

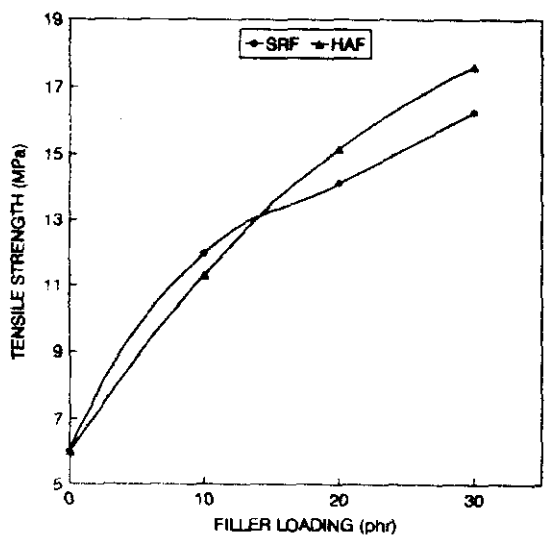

Figure 4.21. Effect of filler loading on tensile strength of $N_{50}P$

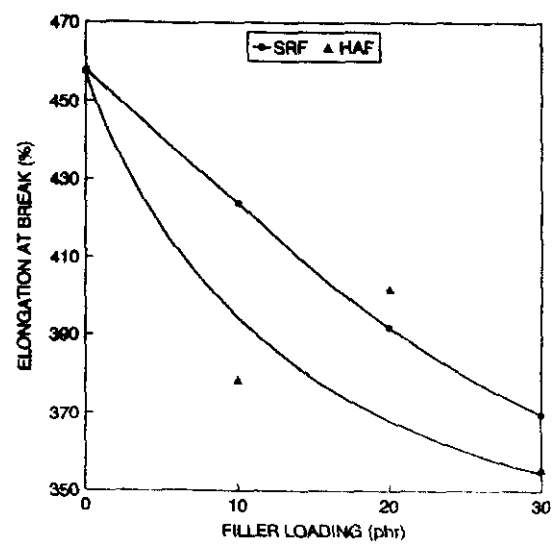

Figure 4.22. Effect of filler loading on elongation at break of $N_{50}P$

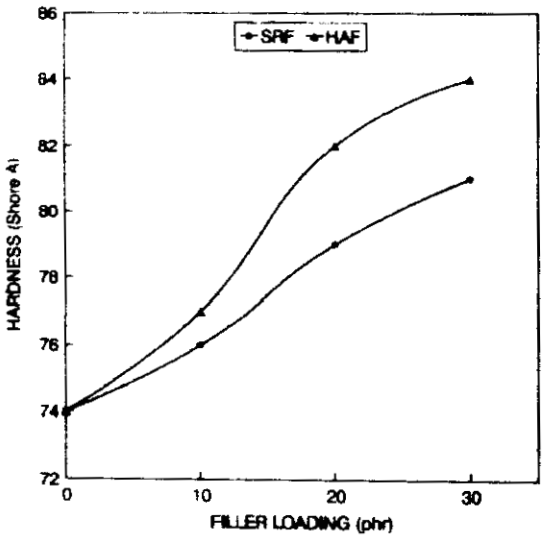

Figure 4.23. Effect of filler loading on hardness of $N_{50}P$

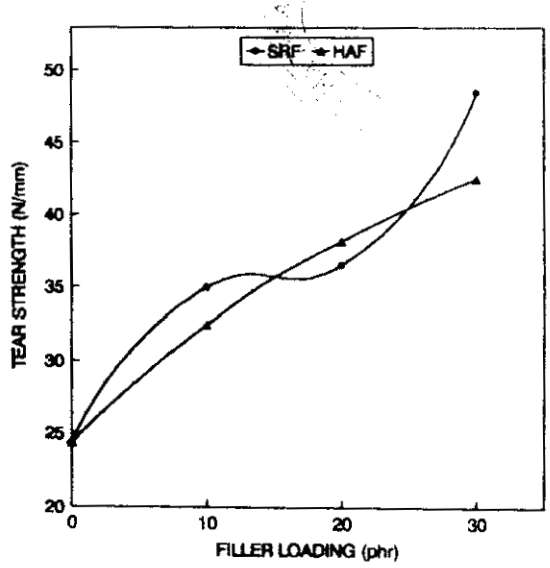

Figure 4.24. Effect of filler loading on tear strength of $N_{50}P$

The load vs. displacement curves of filled NBR/EVA blends are shown in Figures 4.25 and 4.26. The tearing force is lowest for the clay filled system and increases as follows: clay < SRF < silica < HAF (Figure 4.25). The tearing force is also in accordance with the reinforcing ability of the fillers (Figure 4.18). As the filler loading is increased the tearing force is also increased (Figure 4.26).

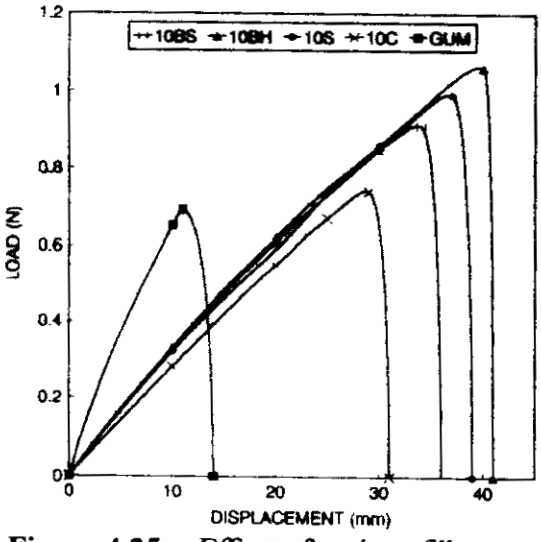

Figure 4.25. Effect of various fillers on the load-displacement curves of NBR/EVA blends

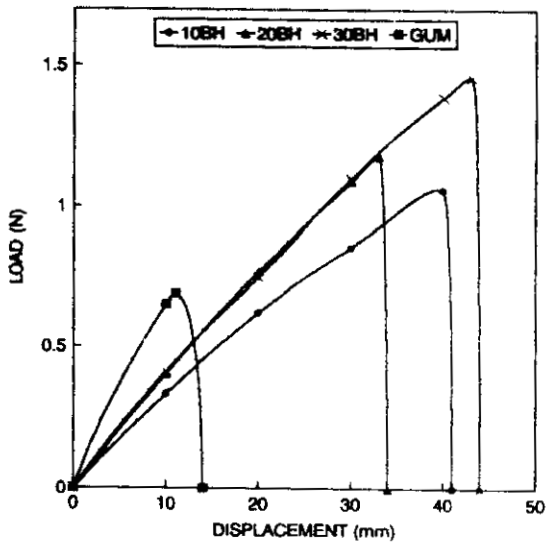

Figure 4.26. Effect of filler loading on the load-displacement curves of $N_{50}P$

(c) Scanning electron microscopic studies

Figures 4.27a–4.27d are the tensile fractographs of various filled systems. In the case of (Figure 4.27a) the silica filled system dewetting of the filler particles is observed. In the clay filled system (Figure 4.27b) also, the dewetting phenomena is observed. But the number of filler particles on the surface is less due to the low reinforcing ability of clay as compared to that of silica. In the case of black filled systems, the dewetting is less predominant for HAF filled system (Figure 4.27d) compared that of SRF filled system (Figure 4.27c). This results from the high reinforcing ability of HAF.

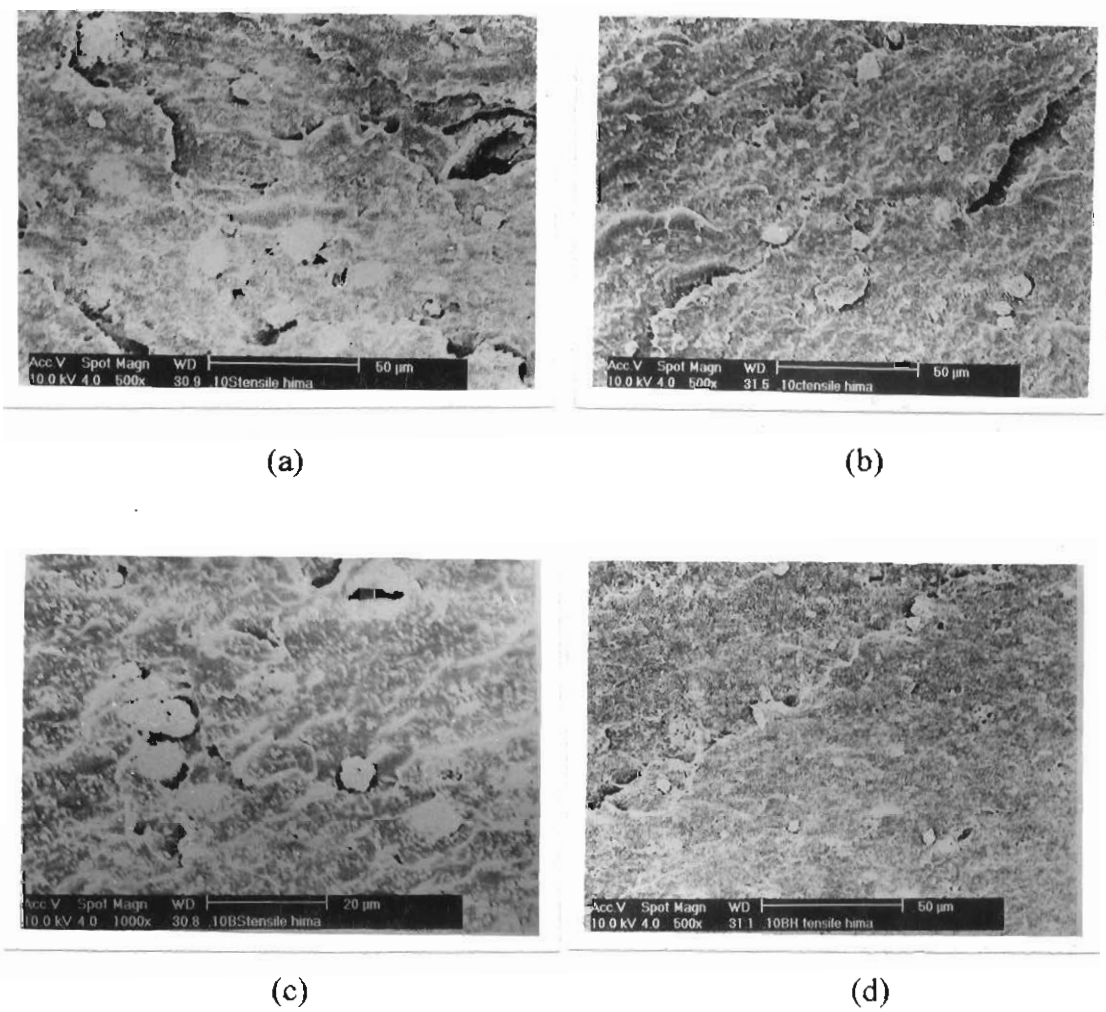

Figure 4.27. Scanning electron micrographs showing the tensile fracture surfaces of (a) 10S (b) 10C (c) 10BS and (d) 10BH

The tear fracture surfaces of filled $N_{50}P$ are shown in Figure 4.28. In the silica filled system (Figure 4.28a) crack deviation is observed due to the restriction to crack propagation by filler particles. The clay filled system (Figure 4.28b) also exhibits the crack deviation, but to a lesser extent compared to silica filled system. In the black filled compounds (Figures 4.28c and 4.28d) the fracture surfaces show crack deviation along with parabolic tear lines distributed randomly. The parabolic tear line results from the interaction of main fracture fronts with subsidiary fracture fronts and from the restriction to tear propagation by filler particles.

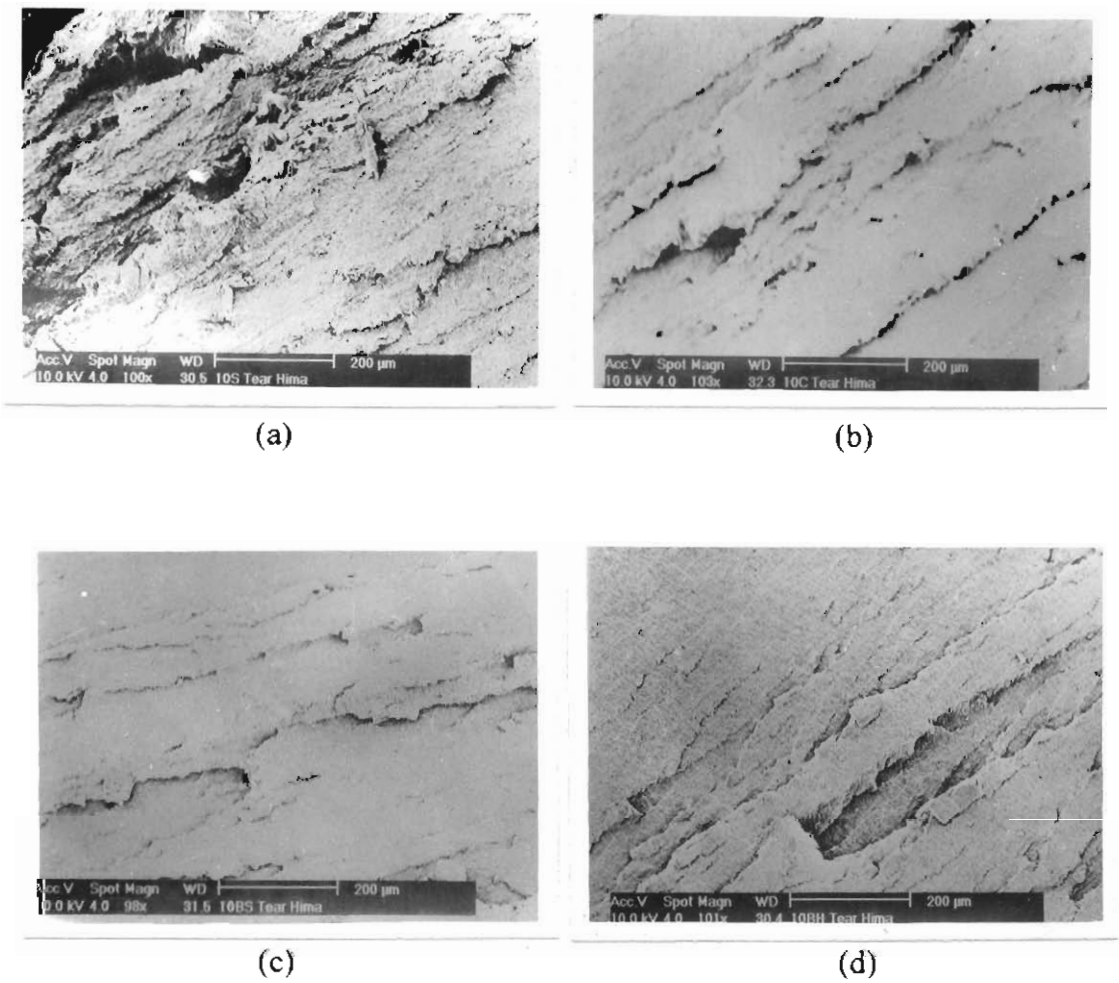

Figure 4.28. Scanning electron micrographs showing the tear fracture surfaces of (a) 10S (b) 10C (c) 10BS and (d) 10BH

(d) Model fitting

The simplest theoretical equation for the reinforcement of a material or the increase in rigidity due to a filler is attributed to Einstein.[23,24] The Einstein equation, valid only at low concentration of filler when there is perfect adhesion between the phases, is given as

$$G = G_1 (1 + 2.5 \phi_2) \tag{4.6}$$

where G is the modulus of the filled system; G_1, the modulus of the unfilled system; ϕ_2, the volume fraction of the filler.

Einstein's equation implies that the stiffening or reinforcing action of a filler is independent of the size of the filler particles. This equation shows that the volume occupied by the filler is independent of the size of the filler particles and it is the volume occupied by the filler rather than weight, that is the important variable. The equation also assumes that filler is very much rigid than the matrix.

An extension of Einstein's theory, originally developed to explain rubber reinforcement, is due to Guth[24] and Smallwood.[23] Their equation for the increase in modulus due to a rigid spherical filler is:

$$G = G_1(1 + 2.5 \phi_2 + 14.1 \phi_2^2) \tag{4.7}$$

Kerner has developed a mathematical theory to describe the reinforcing action of spherical filler particles. The equation due to Kerner is:[25]

$$G = G_1 \left[\frac{\phi_2 G_2 / \left[(7 - 5\nu_1)G_1 + (8 - 10\nu_1)G_2\right] + \phi_1 / 15(1 - \nu_1)}{\phi_2 G_1 / \left[(7 - 5\nu_1)G_1 + (8 - 10\nu_1)G_2\right] + \phi_1 / 15(1 - \nu_1)} \right] \tag{4.8}$$

Many fillers are more rigid than matrices, so that Kerner's equation simplifies to:

$$G = G_1 \left[1 + \frac{\phi_2}{\phi_1}\left(\frac{15(1-\nu_1)}{8-10\nu_1}\right)\right] \qquad (4.9)$$

where ϕ_1 and ϕ_2 are the volume fraction of polymer and filler respectively and ν_1 is the Poisson's ratio.

The suitability of different models to fit modulus data for the HAF filled system is presented in Figure 4.29. It is observed that the experimental values are higher than theoretically predicted ones for all the filler loadings. This indicates a strong interaction between HAF and the blend system. This is also supported by the SEM fractographs shown in Figure 4.27d.

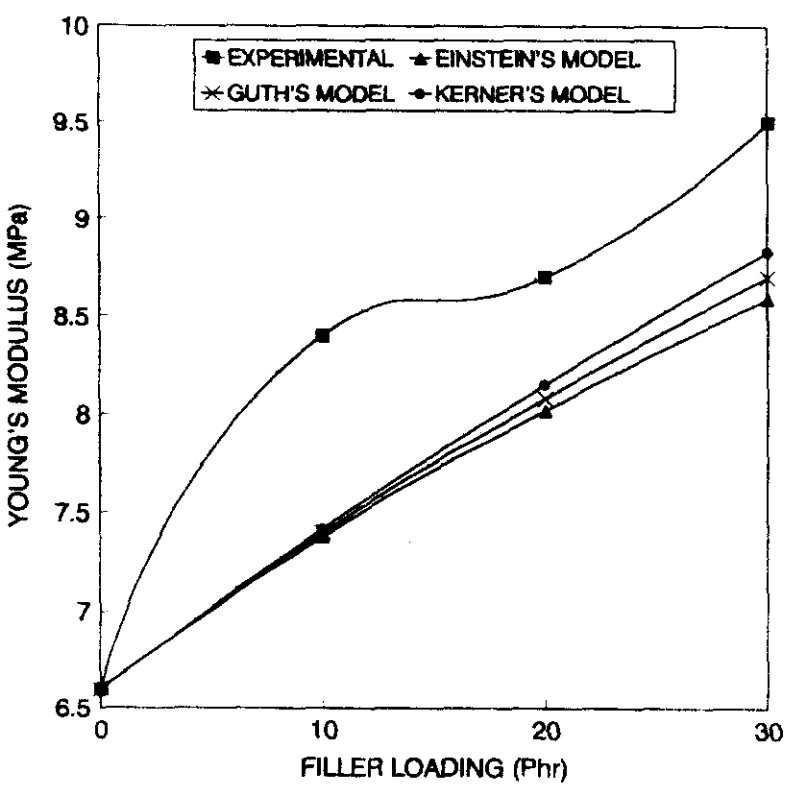

Figure 4.29. Applicability of various models on the Young's modulus of HAF filled $N_{50}P$

4.2 References

1. A S Hay, *Polym. Eng. Sci.*, **16(1)**, 1 (1976)
2. T Nishi and T. T. Wang, *Macromolecules* **8 (6)**, 909 (1976).
3. R L. Imken, D R Paul and Barlow, *Polym. Eng. Sci.*, **16(9)**, 593 (1976).
4. M H. Walters and D. N. Keyte, *Rubber Chem. Technol.*, **38(1),** 62 (1965).
5. R F. Baner and E. A Dudley, *Rubber Chem. Technol.*, **55**, 537 (1982).
6. V A Shershnev, *Rubber Chem. Technol.*, **55**, 537 (1982).
7. J. E. Callan, W. M. Hess and C. E. Scott, *Rubber Chem. Technol.*, **44**, 814 (1971).
8. M. M. Chappuis, M. H. Polley and R. A. Schulz, *Rubber Chem. Technol.*, **28**, 253 (1955).
9. W M Hess, P. C. Vegvari and R. A. Swor, *Rubber Chem. Technol.*, **58**, 350 (1985).
10. W. M. Hess, R. A. Swor and P. C. Vegvari, *Kautsch. Gummi Kunstst.*, **38**, 1114 (1985).
11. S Cimmino, L. Dorazio, R. Greco, G. Maglio, M. Malinconico, C. Mancarella, E Martuscelli, R. Palumbo and G. Ragosta, *Polym. Eng. Sci.*, **24**, 48 (1984).
12. R. Greco, C. Mancarella, E. Martuscelli, G. Ragosta and Yin Jinghua, *Polymer*, **28**, 1929 (1987).
13. G. D. Choi, S. H. Kim and W. H. Jo, *Polym. J.*, **28**, 527 (1996).
14. R. Bagheri and R. A. Pearson, *J. Mater. Sci.*, **31**, 3945 (1996).
15. A N. Gent and C. T. R. Pulford, *J. Mater. Sci.*, **19**, 3612 (1984).
16. B. Kuriakose and S. K. De, *J. Mater. Sci.*, **20**, 1864 (1985).
17. S. S. Bhagawan, D. K. Tripathy and S. K. De, *J. Mater. Sci.*, **6**, 157 (1987).
18. S. Thomas, B. Kuriakose, B. R. Gupta and S. K. De, *J. Mater. Sci.*, **21**, 711 (1986).
19. S. Thomas, B. R. Gupta and S. K. De, *J. Vinyl Technol.*, **9,** 71 (1987).
20. Y Fukahori, *Intl. Polym. Sci. Technol.*, **T/76**, 9 (1982).
21. B M Walker, C. P Rader (Eds.), *Hand Book of Thermoplastic Elastomers,* Van Nostrand Reinhold Company, New York, (1988).
22. G Kraus, *J. Appl. Polym. Sci.*, 7, 861 (1963).
23. H M. Smallwood, *J. Appl. Phys.*, **15**, 758 (1944)
24. E Guth, *J. Appl. Phys.*, **16**, 20 (1945).
25. H Kerner, *Proc. Phys. Soc.*, **69B**, 808 (1956).